RSC Advances

ROYAL SOCIETY OF CHEMISTRY

www.rsc.org/advances

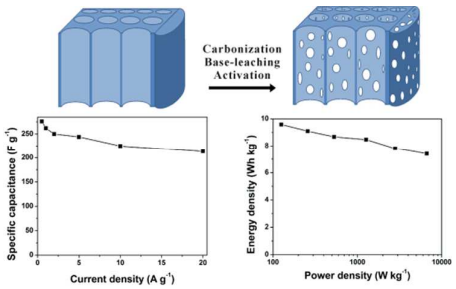

Hierarchical porous carbon based on the self-template structure of rice husk was prepared for high-performance supercapacitors

RSC Advances

RSCPublishing

PAPER

Hierarchical porous carbon based on the self-template structure of rice husk for high-performance supercapacitors†

Cite this: DOI: 10.1039/x0xx00000x

Received 00th January 2012,
Accepted 00th January 2012

DOI: 10.1039/x0xx00000x

www.rsc.org/

Dechen Liu,[a] Wenli Zhang,[a] Haibo Lin,[*ab] Yang Li,[a] Haiyan Lu[*a] and Yan Wang[a]

Using the self-template structure of rice husk (RH), hierarchical porous carbon with high surface area was prepared by carbonization, NaOH-leaching and KOH activation. The formation processes of hierarchical porous structure were discussed in detail, where silica in RH plays a crucial role. The rice husk-based hierarchical porous carbon (RHHPC), with a 3D porous structure, was composed of macrochannels, mesopores and micropores both in its surface and inner channels. The RHHPC exhibited a surface area as high as 2804 m^2 g^{-1} and a high-level oxygen-containing groups (with an oxygen content of 9.74 at %). The high surface area, large amount of oxygen-containing groups and unique hierarchical porous structure endow the RHHPC with a high capacitance (278 F g^{-1} at 0.5 A g^{-1}) and excellent rate capability (77.2% retention at 20A g^{-1}) in 6 mol L^{-1} KOH. Furthermore, the symmetric supercapacitor fabricated with RHHPC delivered a high energy density of 7.4 Wh kg^{-1} at a power density of 6195 W kg^{-1}, which reveals the promising application of RHHPC in high-performance supercapacitors.

1. Introduction

Supercapacitors have received considerable attention because of their high power density, fast recharge capability and long cycle life.[1-3] Porous carbon materials are considered to be the most promising electrode materials for supercapacitors owing to their excellent physicochemical stability, high surface area, good electrical conductivity, and low cost.[4,5] The ideal porous carbon materials should have both high capacitance and good rate capability for the supercapacitors to possess both high energy density and high power density.[6] But, conventional porous carbon usually consists of a single kind of pore, which is difficult to exhibit high capacitance and good rate capability, simultaneously.[7,8] Recently, hierarchical porous carbons(HPCs), with 3D structures composed with macropores, mesopores and micropores are strongly recommended for the fabrication of advanced supercapacitors. Hierarchical porous carbons exhibit the advantages of macropores, mesopores and micropores through a synergistic effect, so it can afford both high capacitance and good rate capability.[9-13] The template with special structure usually is used to fabricate hierarchical porous carbons.[12-15] However, the preparation of template is complicated, expensive, and time-consuming. This restricts their commercial viability. Recently, some novel strategies (for example, co-assembly and self-template methods) for the synthesis of hierarchical porous carbon were proposed to simplify the preparation of template or avoid using template.[16,17] Among, the self-template method for preparing hierarchical porous carbon have been widely investigated using natural biomass material, such as banana peel, watermelon, hemp fiber, bacterial fiber, fish scale, human hair and so on.[18-23] Natural biomass materials exhibit a fine structure which cannot be achieved through artificial synthesis merely. These fine structure of the natural biomass can be transformed into hierarchical porous structure. Besides, the utilization of renewable biomass to produce HPCs is critical to the sustainable development and environmental protection. Although HPCs have been prepared from various biomasses by many researchers, the shortage of raw material is one of the biggest obstacles for their application. Considering the extensive applications of supercapacitors, the development of HPCs from low-cost and abundant biomass could be very rewarding and competitive.

Rice husk (RH) is a kind of low-cost and abundant biomass. The annual world production of RH is approximately 140 million tons.[24] RH possesses unique organized structures and composition (silica). The vascular bundles in RH are natural macroporous channels used to transport water and nutrients for the growth of rice.[25] The silica with unique 3D nano-structure as a natural template skeleton is distributed in RH.[26] Obviously, the self-construction (with both macroporous

vascular bundles and 3D nano-silica) of RH is a natural template structure. If hierarchical porous carbons are prepared by using the self-template structure of RH, it will realize the "template-free" preparation of hierarchical porous carbons. More importantly, this strategy is simple, low-cost and sustainable for large scale industrial production. In recent years, RH has been used to prepare porous carbon via traditional physical and chemical activation methods.[27] Unfortunately, the self-template structure of RH is not fully utilized during preparation process. Namely, the prepared porous carbon does not simultaneously exhibit high specific surface area and hierarchical porous structure. The porous carbon prepared by traditional physical activation exhibits low specific surface area.[28,29] Although the specific surface area of porous carbon is improved via traditional chemical activation, the pore size of prepared porous carbon exhibits narrow micropore-dominated distribution,[30-32] which restricted its application in the supercapacitors with high power performance. Therefore, it is necessary to prepare porous carbon with high specific area and hierarchical porous structure via a novel method in which the self-template structure of RH is transformed into hierarchical porous structure and high specific area is obtained.

In this work, rice husk-based hierarchical porous carbon (RHHPC) with high specific surface area was prepared based on the self-template structure of RH via carbonization, NaOH-leaching and KOH activation. The as-obtained RHHPC maintained the structure of RH with 3D porous surface, parallel porous channels and displayed a specific surface area as high as 2804 $m^2 g^{-1}$, and a high-level oxygen-containing groups(with an oxygen content of 9.74 at %). Benefiting from the high specific surface area, large amount of oxygen-containing groups and unique hierarchical porous structure, the RHHPC exhibited high capacitance and excellent rate performance, which endows RHHPC with great potential in for high-performance supercapacitors.

2. Experimental

2.1 Materials

RH was obtained from a rice mill nearby Changchun city. All other chemical reagents used in this study were of analytical grade from Beijing Chemicals Co., Ltd. Nitrogen was of chemical grade (purity of 99%). Deionized water was used throughout the experiment.

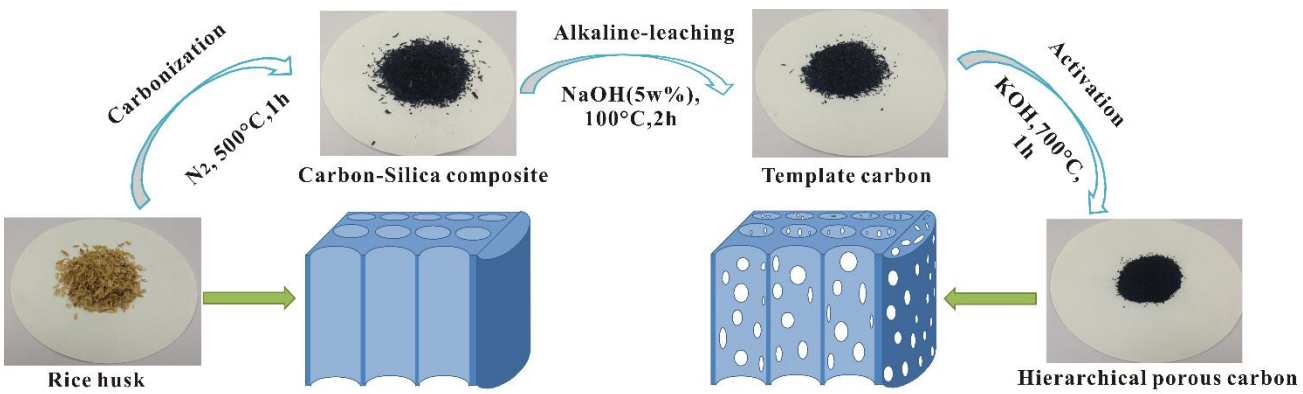

Fig. 1 Schematic of the preparation of RHHPC.

2.2 Preparation of RHHPC

The main processes of preparing RHHPC are schematically illustrated in Fig. 1. The RH was heated to 500 ℃ and pyrolyzed for 1 h in a tubular furnace under the protection of nitrogen, then the carbon-silica composite was obtained. The carbon-silica composite was treated with NaOH-leaching, namely, the carbon-silica composite was refluxed with a solution of 10 wt% NaOH at 100 ℃ for 2h to gain template carbon, then the template carbon was added to KOH solution to obtain the mixture with a KOH-to-template carbon ratio of 4:1 by weight. Next, the mixture was dried at 110 ℃ to obtain the KOH-impregnated template carbon. The KOH-impregnated template carbon was heated up to 700 ℃ for 1h in an electrical furnace. The activated mixtures were washed with deionized water until the filtrate became neutral. The sample was finally dried overnight at 100 ℃.

2.3 Characterizations of RHHPC

The porous characteristics of the prepared materials were measured by N_2 adsorption at 77 K using an ASAP 2010 Micrometrics instrument. The specific surface area was calculated on the basis of the Brunauer–Emmett–Teller (BET) model, and the pore size distribution (PSD) was calculated from desorption branch isotherms by the Density Functional Theory. The pore volume was estimated from the adsorbed amount at a relative pressure (P/P_0) of about 0.97. The morphologies and structural properties of the prepared materials were characterized by field emission scanning electron microscopy (FESEM; HITACHI SU8020) and transmission electron microscopy (TEM, JEOL, JEM 1200EX). The structural properties were investigated by X-ray diffraction (XRD, Rigaku D/max 2550), Raman spectra (Bruker VERTEX 70). The X-ray

photoelectron spectroscopy (XPS) analysis was performed on the Thermo VG ESCALAB250 surface analysis system.

2.4 Electrochemical measurements

The electrochemical performances of the electrodes were measured in two-electrode setup. Each electrode was composed of 85 wt% of RHHPC, 10 wt% of acetylene black and 5 wt% of polytetrafluoroethylene. The electrochemical characteristics of samples were determined by galvanostatic charge/discharge (GCD), cyclic voltammetry (CV), and electrochemical impedance spectroscopy (EIS) in 6M KOH. GCD was carried out on an NEWARE-BTS4008 test station at different current densities from 0.5 A g^{-1} to 20 A g^{-1}, with the voltage window from 0 to 1 V. The PARSTAT 2273 electrochemical system was used for CV and EIS measurements. CV was conducted between 0 and 1 V at increasing sweep rates from 5 to 1000 mV s^{-1}. EIS measurement was conducted at 0 V by sweeping the frequencies from 100 kHz to 0.1 Hz range with a voltage amplitude of 10 mV.

3. Results and discussion

The RHHPC was prepared via carbonization, NaOH-leaching and KOH activation. Each process is a great need to obtain hierarchical porous structure from the self-template structure of RH.

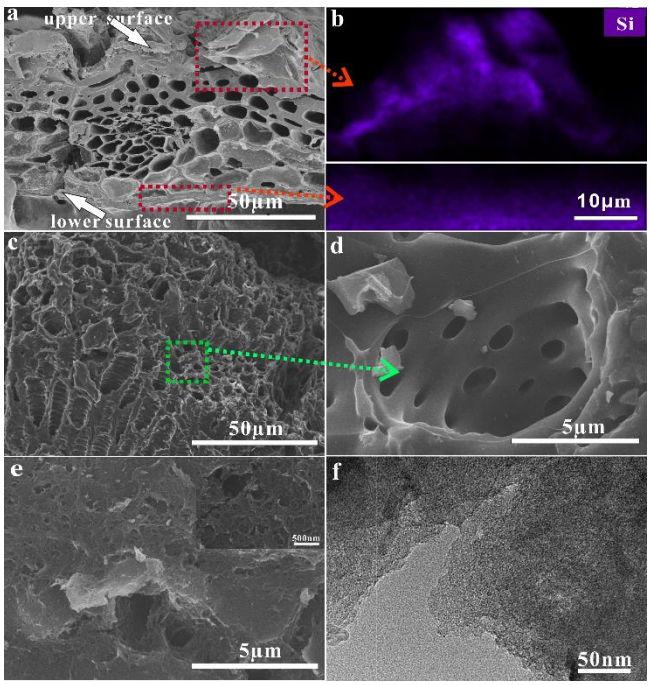

Fig. 2 (a) SEM image of carbon-silica composite cross section; (b) Si-mapped SEM-EDS image; (c) SEM image of the cross section of RHHPC; (d) high-magnification SEM image of parallel vascular bundle in RHHPC; (e) SEM image of surface of RHHPC (Inset) high-magnification SEM; (f) TEM image of RHHPC.

In the process of carbonization, the organic components of RH were pyrolyzed to form a stable porous structure. As shown in Fig. 2a, the self-construction of RH was perfectly preserved during carbonization process. Especially, the vascular bundles with channels from 2 to 10 μm were preserved very well as they appear in RH (see Supporting Information†, Fig. S1). Meanwhile, a carbon-silica composite with nano-silica distributed in the upper and lower surface (the upper surface is the outer epidermis of rice husk and the lower surface is the inner epidermis of rice husk, Fig. S2†) was obtained in carbonization process (Fig. 2b). The obtained carbon-silica composite exhibited a low specific surface area of 19 m^2 g^{-1} (Table S1†) owing to small amount of pore developed in carbonization process.

In order to utilize the self-template structure of RH, the carbon-silica composite was treated by NaOH-leaching. The nano-silica of carbon-silica composite was removed by NaOH, and the 3D nano-structure of silica was mapped in carbon matrix of the upper and lower surface. So, the template carbon with 3D structure on surface and inner parallel vascular bundles was obtained. The specific surface area of template carbon was increased to 247 m^2 g^{-1} (Table S1†), which is much larger than that of carbon-silica composite. Although template carbon has unique structure, it suffers from low specific area leading to low capacitance.

The template carbon was activated by KOH for gaining hierarchical porous carbon with high specific surface area. The vascular bundles of RHHPC were still perfectly preserved after KOH activation (Fig. 2c). Besides, the relatively smaller macropores with pore diameter of 100-500 nm were clearly observed in the vascular walls (Fig.2d). The surface of RHHPC exhibited 3D porous structure with different pore size (Fig. 2e). In addition, a large amount of micropores and mesopores were observed in RHHPC (Fig. 2f).

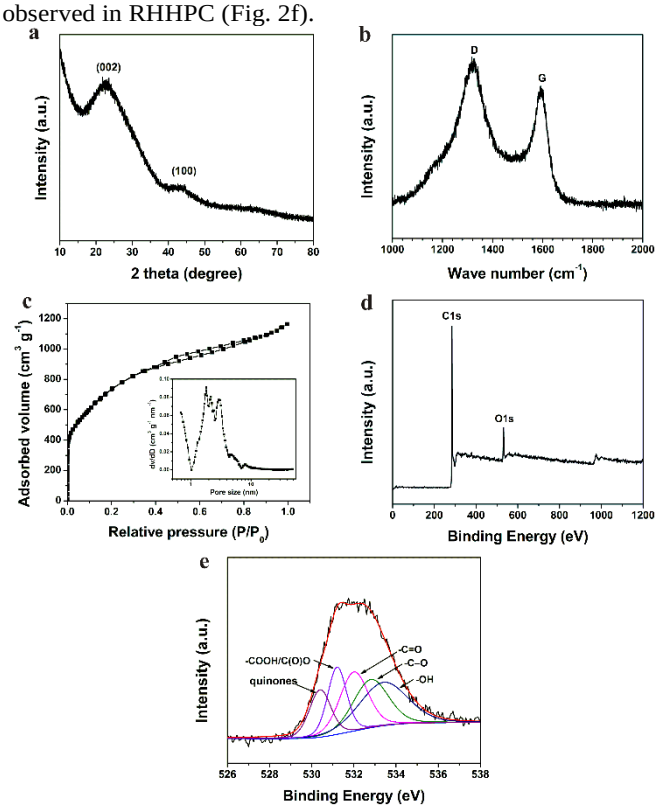

Fig. 3 (a) XRD patterns, (b) Raman spectra, (c) Nitrogen adsorption–desorption isotherms and pore size distribution (the inset), (d) XPS survey spectrum and (e) high resolution O1s XPS spectrum of RHHPC.

XRD and Raman spectroscopy were carried out to determine the structure of RHHPC. The broad peaks at approximately 22.5 and 43 ° in Fig. 3a, which can be attributed to typical reflections from the (002) and (100) planes of graphite, implies the amorphous structure of RHHPC.[33] The two characteristic peaks at around 1330 and 1590 cm^{-1} exhibited in the Raman spectra (Fig. 3b) corresponded to the D-band (disordered carbon) and G-band (ordered graphite lattice), respectively.[34,35] Besides, the ratio of the relative intensity of these two bands (I_D/I_G) is proportional to the number of defect sites in the graphite carbon.[36,37] The lower the ratio is, the higher the graphitization is. It can be calculated that the I_D/I_G ratio of RHHPC is 1.26. The result confirmed that RHHPC has low graphitization degree. The low graphitization degree of RHHPC may be caused by the harsh KOH activation and doping of oxygen.

N_2 adsorption–desorption isothermal analysis was performed to characterize the porous structures of RHHPC. RHHPC showed a combined I/IV type adsorption–desorption isothermal indicating that micro-, meso- and macropores coexist in RHHPC (Fig. 3c). A strong N_2 adsorption occurs at low relative pressure of less than 0.1 due to the presence of micropores. The obvious hysteresis loop between the adsorption and desorption branches (at 0.4-0.8 P/P_0) suggests the existence of mesopores. This result was in accordance with the PSD (insert of Fig. 3c). The PSD of RHHPC extended over the micropore and mesopore range, which is in good agreement with the observation results obtained by TEM. In addition, the slightly steep adsorption at the relative pressure of 0.8-1.0 demonstrated the presence of macropores. Calculated by the Brunauer–Emmett–Teller (BET) model, the specific surface area of RHHPC was as high as 2804 $m^2\ g^{-1}$ with a pore volume up to 1.797 $cm^3\ g^{-1}$. Such a high specific surface area can provide a sufficient electrode-electrolyte interface for the accumulation of ions. The surface chemistry of RHHPC was evaluated by XPS. The obvious C1s and O1s peaks were observed in the XPS spectra (Fig. 3d). The high-resolution O1s spectrum of RHHPC (Fig. 3e) can be deconvoluted into five individual component peaks corresponding to quinone type groups (530.4 eV), COOH/C(O)O (531.2 eV), C=O (531.9 eV), –C–O (532.8 eV) and –OH (533.4 eV).[38] The contents of individual oxygen-containing functional groups in RHHPC were summarized in Table S2†. The total surface oxygen content of RHHPC was 9.7 at%, showing the abundant oxygen-containing functional groups in the RHHPC. These oxygen-containing groups contribute to pseudo-Faradaic reactions and enable easy access of electrolyte species for the construction of double layer.[39,40]

From the above results, it can be concluded that the RHHPC has the unique features such as hierarchical porous structure, high specific surface area and large amount of oxygen-containing groups. These unique features would endow RHHPC with excellent electrochemical performance.

Obviously, compared with porous carbon with dominant micropore derived from RH via traditional method, the obtained RHHPC exhibited hierarchical porous structure in our work. We believe that the development of hierarchical porous structure is related to the utilization of self-template structure of RH and the removal of silica. To clarify this, Rice husk carbon (RHC) was prepared through traditional KOH activation process with the same annealing conditions as RHHPC (detailed in Supporting Information).

The obtained RHC exhibited irregular bulks rather than keeping the self-template structure of RH (Fig. S3†). The adsorption-desorption isotherm of RHC is approximately I type isotherm (Fig. S4†).[41] It indicates that RHC possesses the high microporosity, which was different from RHHPC. This result is proved by pore size distribution of RHC (Fig. S5†).The reason is that the KOH reacts with silica on the upper and lower epidermis of RH and the new-born silicate generated from silica and KOH hinder the activation process.[42] The process of forming macropores and mesopores structure from the 3D nano-structured carbon skeleton (due to the existence of nano-silica in the upper and lower surface of RH) by KOH etching was inhibited by defect activation. Meanwhile, this caused excessive etch and damage in the vascular bundles structure of carbon-silica composite. In consequence, the self-template structure of RH was not fully utilized in developing hierarchical porous structure via traditional KOH activation process.

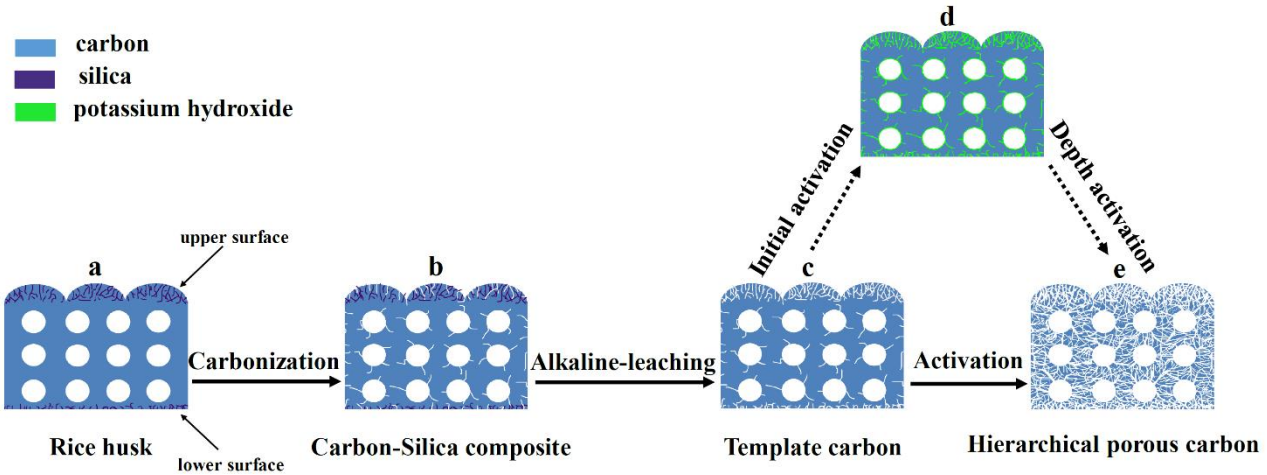

Fig. 4 Schematic illustration of the formation process of hierarchical porous structure in RHHPC

Based on the above analysis, we proposed an explanation for how such hierarchical porous structure was formed. The formation process of hierarchical porous structure in RHHPC is shown in Fig. 4. In carbonization process, the carbon–silica composite with low specific surface area (Fig. 4b) was obtained due to the destruction of cellulose and hemicellulose in RH and the evaporation of volatile material in carbonization process.[43] In NaOH-leaching process, template carbon (Fig. 4c) with 3D structure in surface (both upper and lower) and inner parallel vascular bundles was formed due to the removal of nano-silica in carbon-silica composite. The unique structure of template carbon was gradually transformed into hierarchical porous structure during KOH activation (detailed process as shown in Fig. 4c to 4d to 4e). At the beginning of KOH activation, active metallic potassium congregated in the porous channel of nano-structured carbon in surface and vascular bundles via capillary interaction (Fig. 4d).[44] Along with the activation, the primary porous channels were enlarged forming macropores and large amounts of micropores and mesopores were formed in these macropores. When the activation reaction increased to some extent, the unconnected pores were interconnected. The hierarchical porous structure was obtained (Fig. 4e).

In order to verify the effectiveness of RHHPC as new electrode material for supercapacitors, CV, GCD, and EIS were measured in a 6 M KOH aqueous electrolyte.

Fig. 5a presents the CV curves of RHHPC electrode at different scan rates from 5 to 1000 mV s^{-1}. Notably, the quasi-rectangular shape of CV curves were well kept at a large range of scan rates and still exhibited a well symmetric shape even at 1000 mV s^{-1}, indicating ideal double-layer capacitive properties. Fig. 5b shows the GCD curves for the RHHPC at different current densities. The GCD curves were nearly symmetric triangular shapes, indicating excellent capacitive behaviour. The gravimetric specific capacitance values at different current densities are shown in Fig. 5c. The corresponding specific capacitances of the electrode are calculated on the basis of the following equation:

$$C = \frac{I\Delta t}{2m\Delta V} \times 4 \quad (1)$$

where I is the discharge current (A), Δt is the total discharge time (s), m is the mass of single electrode (g) and ΔV is the potential difference (V) in the discharge process. The calculated specific capacitance of RHHPC was as high as 278 F g^{-1} at 0.5 A g^{-1} owing to the high specific surface area of RHHPC with a large amount of oxygen-containing groups. It should be noted that the RHHPC still exhibited a relative high specific capacitance of 213F g^{-1} with a retention of 77.2% at a high current density of 20.0 A g^{-1}. Obviously, the RHHPC exhibited excellent rate capability. The performance of the RHHPC is better than those of most of the activated carbons derived from other biomass (chicken feather, bagasse, enteromorpha prolifera, endothelium corneum gigeriae galli) shown in Table S3†.[1,45-47] Furthermore, a microporous RHC for supercapacitor was measured as well for comparison, as depicted in Fig. S6†. For microporous RHC electrode, the specific capacitance decreased from 315 to 163 F g^{-1} as the current density increased from 0.5 to 20 A g^{-1}. The capacitance retention is ca. 50% which is lower than that of RHHPC. This confirms that the unique hierarchical porous structure in RHHPC is helpful for ion diffusion at high current density.

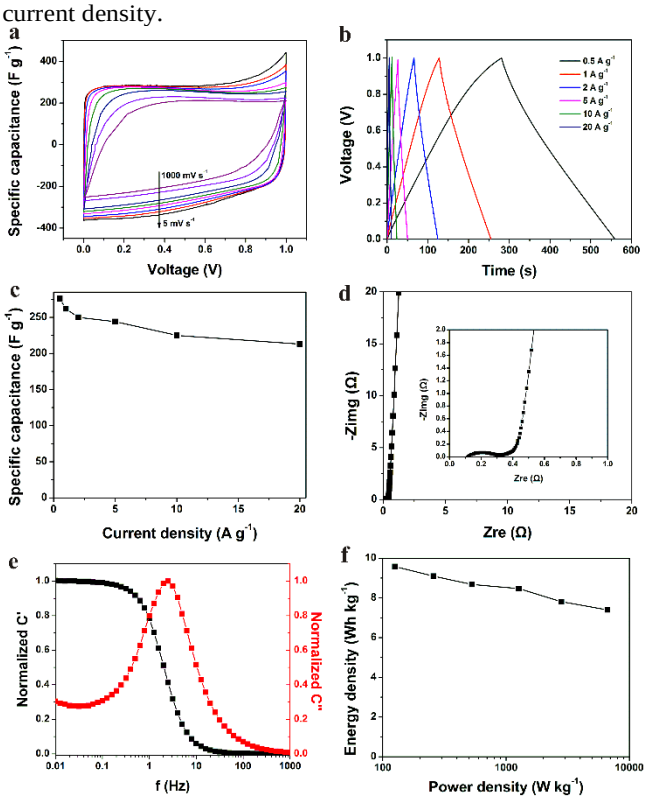

Fig. 5 Electrochemical performances of RHHPC measured in 6 M KOH aqueous solution: (a) CV curves at various scan rates and (b) charge/discharge curves at various current densities within a voltage range of 0 to 1 V; (c) specific capacitance as a function of current density ranging from 0.5 to 20 A g^{-1}; (d) the Nyquist plot with frequency ranging from 100 kHz to 0.1 Hz; (e) the normalized real and imaginary part capacitance as a function of frequency; (f) Ragone plot of the RHHPC//RHHPC symmetric supercapacitor.

Fig. 5d shows the Nyquist plot based on a frequency response analysis of frequencies ranging from 0.01 Hz to 100 kHz. At low frequencies, the straight line tends to be perpendicular to the real axis, indicating the capacitive behavior.[17] There is a semicircle on the impedance plot of RHHPC at high frequency (inset in Fig. 5d). The diameter of the semicircle along the real axis represents the charge-transfer resistance at the contact interface between the carbon and electrolyte in the pores of the electrode.[8,48] A small semicircle indicated a low charge-transfer resistance. This is due to that the hierarchical porous structure of RHHPC and abundant oxygen-containing functional groups increase pore accessibility for the electrolyte. A small x-intercept (low equivalent series resistance (ESR)) was also observed for RHHPC in the high frequency region (inset in Fig. 5d). The ESR arises from the intrinsic electronic properties of the electrode matrix and electrolyte solution, mass transfer resistance of the ions in the matrix, and contact resistance between the current collector and the electrode.[49,50] Such a low ESR of RHHPC is mainly due to the low contact resistance between the ion and material (where

interconnected ion channels facilitate contact between the ion and material), and is also attributable to the good intrinsic electronic properties of the material.[12] These results prove that the unique hierarchical porous structure can facilitate rapid electron and ion transport.[51]

The impedance frequency behavior was further investigated by the complex model of the capacitance (C(w)). The normalized C'(w) and C"(w) as a function of frequency for the RHHPC electrodes are presented in Fig. 5e. It is obvious that the C'(w) is increased with the decrease of frequency, which can be attributed to the transformation from resistive behavior to capacitive behavior of RHHPC. In addition, the characteristic relaxation time constant defined as $\tau_0 = 1/f_0$ (τ_0, the minimum time to discharge all of the energy from a device with an efficiency of more than 50%[52]) is obtained from the frequency (f_0) where C"(w) is the maximum. The f_0 is 2.51 Hz, corresponding to a τ_0 of 398 ms. This result further demonstrates the fast accessibility of the RHHPC electrode to the electrolyte ions, the enhanced electrical conductivity and the excellent rate capability at high scan rates with high power density characteristics.

The energy density (E) and the power density (P) are important parameters to characterize the electrochemical performance of supercapacitor. Fig. 5f shows the Ragone plot of the symmetric supercapacitor based on the RHHPC electrodes. The energy density and power density can be calculated based on the following equations:

$$C_T = \frac{1}{4}C \quad (2)$$

$$E = \frac{1}{2}C_T V^2 \quad (3)$$

$$P = \frac{E}{\Delta t} \quad (4)$$

where C_T is the specific capacitance of the symmetric supercapacitor calculated according to galvanostatic charge/discharge curves based on the total mass of two electrodes (F g^{-1}), V is the voltage range (V) and Δt is the discharge time (s).

As shown in Fig. 5f, with the increase of power density, energy density decreased slowly. When the power density increased from 125 to 6195 W kg^{-1}, the energy density decreased from 9.6 to 7.4 Wh kg^{-1}. Based on the above results, it can be concluded that RHHPC electrode is capable of delivering high power without profound loss in energy, indicating a promising application in electrochemical capacitors. Furthermore, the cycling performance of RHHPC was investigated for as long as 6000 charge/discharge cycles. Fig. S7† displays the variations in discharge capacitance for the RHHPC electrode as a function of cycle number at a current density of 1 A g^{-1}. As shown in Fig. S7†, the specific capacitance of RHHPC decreased slowly, and about 90.5 % of the initial specific capacitance is retained after 6000 cycles. This demonstrates that the RHHPC has a relatively good long-term stability in the KOH electrolyte.

Such excellent electrochemical performance of RHHPC benefits from its high specific surface area, oxygen-containing groups and unique hierarchical structure. Firstly, high specific surface area affords sufficient electrode–electrolyte interface for the construction of electric double layer. Secondly, the oxygen-containing groups contribute to pseudo-Faradaic reactions and enable easy access of the electrolyte species for the construction of double layer; thirdly, the hierarchical porous nanostructure ensures the fast ion diffusion by shortening the diffusion pathways and using macropores frameworks as ion-buffering reservoirs, mesopores as ion-highways for fast ion transport and micropores for charge accommodation. These electrochemical performances will make the RHHPC material meet the need for high performance supercapacitors with high rate capability and power density.

Conclusions

Herein, we have developed a strategy for the preparation of hierarchical porous carbon from RH by carbonization, NaOH-leaching, and KOH activation, in which hierarchical structure was formed from the self-template structure of RH. The formation process of hierarchical structure in RHHC was proposed, where silica plays a crucial role. The template carbon with 3D structure in surface and inner parallel vascular bundles was obtained by the removal of silica. The unique structure of template carbon was gradually transformed into hierarchical porous structure during KOH activation. The as-obtained RHHPC maintained the structure of RH with 3D porous surface, parallel porous channels. Besides, RHHPC possessed high specific surface area (2804 m^2 g^{-1}). The RHHPC exhibited both a high specific capacitance (278 F g^{-1} at 0.5 A g^{-1}) and excellent rate capability. The energy density of RHHPC based symmetric supercapacitor is as high as 7.4 Wh kg^{-1} even at the power density of 6195 W kg^{-1}. The RHHPC is a promising candidate material for high performance supercapacitors. Moreover, this strategy, using self-structure and component of biomass materials to prepare HPC, can provide new opportunities in developing carbon electrode materials for high-performance supercapacitors.

Acknowledgements

The authors would like to acknowledge the support provided by key project in Jilin Province (20126010).

Notes and references

[a] *College of Chemistry, Jilin University, Changchun 130012, China.*

[b] *Key Laboratory of Physics and Technology for Advanced Batteries of Ministry of Education, Jilin University, Changchun, 130012, China.*

** Corresponding author. Tel.: +86 431 85155189; fax: +86 431 85155189 E-mail address:* lhb910@jlu.edu.cn *(H. Lin),* luhy@jlu.edu.cn *(H. Lu)*

† Electronic Supplementary Information (ESI) available: Detailed preparation process of RHC; Pore structure of RHHPC, RHC, Template carbon and carbon-silica composite; SEM image of RHC; SEM image and digital photograph of RH; Nitrogen adsorption–desorption isotherms of RHC; Summary of oxygen containing functional groups in RHHPC; Pore size distribution of RHC and RHHPC; Relationships between the specific capacitance values and current density for RHC and RHHPC; Comparison of the electrochemical performances of RHHPC and other reported porous carbon materials; Galvanostatic charge/discharge cycling stability of RHHPC.

References

1 P. Hao, Z. H. Zhao, J. Tian, H. D. Li, Y. H. Sang, G. W. Yu, H. Q. Cai, H. Liu, C. P. Wong and A. Umar. *Nanoscale*, 2014, **6**, 12120-12129.

2 J. R. Miller and P. Simon, *Science*, 2008, **321**, 651–652.

3 P. Simon and Y. Gogotsi, *Nat. Mater.*, 2008, **7**, 845–854.
4 Y. S. Tao, M. Endo and K. Kaneko, *J. Am. Chem. Soc.*, 2009, **131**,904–905.
5 L. L. Zhang and X. Zhao, Chem. *Soc. Rev.*, 2009, **38**, 2520–2531.
6 B. Xu, S. S. Hou, G.P. Cao, Mo Chub and Y. S Yang, *RSC Adv.*, 2013, **3**, 17500–17506.
7 L. Qie, W. M Chen, H. H. Xu, X. Q. Xiong, Y. Jiang, F. Zou, X. L. Hu, Y. Xin, Z. L. Zhang and Y. H. Huang, *Energy Environ. Sci.*, 2013, **6**, 2497–2504.
8 H. Zhong, F. Xu, Z. H Li, R. W. Fu and D. C. Wu, *Nanoscale*, 2013, **5**, 4678-4682.
9 F. Xu, R.J. Cai, Q.C. Zeng, C. Zou, D.C. Wu, F. Li, X.E. Lu, Y.R. Liang and R.W. Fu, *J. Mater. Chem.*, 2011, **21**, 1970-1976.
10 D. W. Wang, F. Li, M. Liu, G. Q. Lu and H. M. Cheng, *Angew. Chem., Int. Ed.*, 2008, **47**, 373–376.
11 Y. Guo, Z. Q. Shi, M. M. Chen and C. Y. Wang, *J. Power Sources*, 2014, **252**, 235-243.
12 Y. Y. Li, Z. S. Li and P. K. Shen, *Adv. Mater.*, 2013, **25**, 2474–2480.
13 T. C. Chou, C. H. Huang, R. A. Doong and C. C. Hu, *J. Mater. Chem. A*, 2013, **1**, 2886-2895.
14 Q. Wang, J. Yan, Y. B. Wang, T. Wei, M. L. Zhang, X. Y. Jing and Z. J. Fan, *Carbon*, 2014, **67**, 119–127.
15 Y. Han, X.T. Dong, C. Zhang and S. X. Liu. *J. Power Sources*, 2012, **211**, 92-96.
16 P. K. Tripathi, M. X. Liu, Y. H. Zhao, X. M. Ma, L. H. Gan, O. Noonanb and C. Z. Yu, *J. Mater. Chem. A*, 2014, **2**, 8534-8544.
17 M. J. Li, C. M. Liu, H. B. Cao, H. Zhao, Y. Zhang and Z. J. Fan, *J. Mater. Chem. A*, 2014, **2**, 14844-14851.
18 Y. K. Lv, L. H. Gan, M. X. Liu, W. Xiong, Z. J. Xu, D. Z. Zhu and D. S. Wright, *J. Power Sources*, 2012, **209**, 152-157.
19 X.-L. Wu, T. Wen, H.-L. Guo, S. Yang, X. Wang and A.-W. Xu, *ACS Nano*, 2013, **7**, 3589-3597.
20 H. Wang, Z. Xu, A. Kohandehghan, Z. Li, K. Cui, X. Tan, T. J. Stephenson, C. K. King'ondu, C. M. B. Holt, B. C. Olsen, J. K. Tak, D. Harfield, A. O. Anyia and D. Mitlin, *ACS Nano*, 2013, **7**, 5131-5141.
21 L.-F. Chen, Z.-H. Huang, H.-W. Liang, W.-T. Yao, Z.-Y. Yu and S.-H. Yu, *Energy Environ. Sci.*, 2013, **6**, 3331-3338.
22 W. X. Chen, H. Zhang, Y. Q. Huang and W.Q. Wang, *J. Mater. Chem.*, 2010, **20**, 4773–4775.
23 W. J. Qian, F. X. Sun, Y. H. Xu, L. H. Qiu, C. H. Liu, S. D. Wang and F. Yan, *Energy Environ. Sci.*, 2014, **7**, 379–386.
24 D. Kalderis, S. Bethanis, P. Paraskeva and E, Diamadopoulos. *Bioresour Technol.*, 2008, **99**, 6809-6816.
25 B. D. Park, S. G. Wi, K. H. Lee, A. P. Singh, T. H. Yoon and Y. S. Kim, *Biomass Bioenergy*, 2003, **25**, 319–327.
26 D. S. Jung, M. -H. Ryou, Y. J. Sung, S. B. Park and J. W. Choi, *Proc. Nat. Acad. Sci. USA*, 2013, **110**, 12229-12234.
27 Y. Chen, Y. C. Zhu, Z. C. Wang, Y. Li, L. L. Wang, L. L. Ding, X. Y. Gao, Y. J. Ma and Y. P. Guo, *Adv. Colloid Interfac.*, 2011, **163**, 39-52.
28 C. Deiana, D. Granados, R. Venturini, A. Amaya, M. Sergio and N. Tancredi, *Ind. Eng. Chem. Res.*, 2008, **47**, 4754-4757.
29 S. Kumagai, Y. Shimizu, Y. Toida and Y. Enda, *Fuel*, 2009, **88**, 1975-1982.
30 Y. P. Guo, S. F. Yang, K. F. Yu, J. Z. Zhao, Z. C. Wang and H. D. Xu, *Mater. Chem. Phys.*, 2002, **74**, 320-323.
31 X. J. He, P. H. Ling, J.S. Qiu, M. X. Yu, X.Y. Zhang, C. Yu and M. D. Zheng, *J. Power Sources*, 2013, **240**, 109-113.
32 L. J. Kennedy, J. J. Vijaya and G. Sekaran, *Ind. Eng. Chem. Res.*, 2004, **43**, 1832-1838.
33 W. X. Chen, H. Zhang, Y. Q. Huang and W. K. Wang, *J. Mater. Chem.*, 2010, **20**, 4773-4775
34 A. Jänes, H. Kurig and E. Lust, *Carbon*, 2007, **45**, 1226–1233.
35 F. Bonhomme, J. C. Lassègue and L. Servant, *J. Electrochem. Soc.*, 2001, **148**, 450–458.
36 M. X. Liu, L. H. Gan, W. Xiong, Z. J. Xu, D. Z. Zhu and L. W. Chen, *J. Mater. Chem. A*, 2014, **2**, 2555–2562.
37 M. X. Liu, L. H. Gan, W. Xiong, F. Q. Zhao, X. Z. Fan, D. Z. Zhu, Z. J. Xu, Z. X. Hao, and L. W. Chen, *Energ. Fuel.*, 2013, **27**, 1168-1173.
38 R. Arrigo, M. Havecker, S. Wrabetz, R. Blume, M. Lerch, J. McGregor, E. P. J. Parrott, J. A. Zeitler, L. F. Gladden, A. Knop-Gericke, R. Schlogl and D. S. Su, J. *Am. Chem. Soc.*, 2010, **132**, 9616.
39 W. Li, F. Zhang, Y. Dou, Z. Wu, H. Liu, X. Qian, D. Gu, Y. Xia, B. Tu and D. Zhao, *Adv. Energy Mater.*, 2011, **1**, 382–386.
40 P. J. Hall, M. Mirzaeian, S. I. Fletcher, F. B. Sillars, A. J. R. Rennie, G. O. Shitta-Bey, G. Wilson, A. Cruden and R. Carter, *Energy Environ. Sci.*, 2010, **3**, 1238–1251.
41 L. Qie, W. M. Chen, Z. H. Wang, Q. G. Shao, X. Li, L. X. Yuan, X. L. Hu, W. X. Zhang and Y. H. Huang, *Adv. Mater.*, 2012, **24**, 2047–2050.
42 J. B. Zhang, L. J. Jin, J. Cheng and H. Q. Hu, *Fuel*, 2013, **109**, 2–8.
43 A. Bharadwaj, Y. Wang, S.Sridhar, V. Arunachalam. *Curr. Sci.*, 2004, **87**, 981-986.
44 Y. Y. Lv, F. Zhang, Y. Q. Dou, Y. P. Zhai, J. X. Wang, H. J. Liu, Y. Y. Xia, B. Tu and D. Y. Zhao, *J. Mater. Chem.*, 2012, **22**, 93-99.
45 Q. Wang, Q. Cao, X.Y. Wang, B. Jing, H. Kuang and L. Zhou, *J. Power Sources*, 2013, **225**, 101-107.
46 .Gao, W.L. Zhang, Q.Y. Yue, B.Y. Gao, Y.Y. Sun, J.J. Kong and P. Zhao, *J. Power Sources*, 2014, **270**, 403-410.
47 X. T. Hong, K. S. Hui, Z. Zeng, K. N. Hui, L. J. Zhang, M. Y. Mo and M. Li, *Electrochim. Acta.*, 2014, **130**, 464-469.
48 Y. S. Yun, C. B. Im, H. H. Par, I. Hwang, Y. Tak and H. J. Jin, *J. Power Sources*, 2013, **234**, 285-291.
49 M. M. Shaijumon, F. S. Ou, L. Ci and P. M. Ajayan, *Chem. Commun.*, 2008, **20**, 2373-2375.
50 L. Zhang, F. Zhang, X. Yang, G. K. Long, Y. P. Wu, T. F. Zhang, K. Leng, Y. Huang, Y. F. Ma, A. Yu and Y. S. Chen, *Sci. Rep.*, 2013, **3**, 1408-1446.
51 B. Z. Fang, J. H. Kim, M. S. Kim, A. Bonakdarpour, A. Lam, D. P. Wilkinson and J. S Yu, *J. Mater. Chem.*, 2012, **22**, 19031–19038.
52 P. Banerjee, I. Perez, L. Henn-Lecordier, S. B. Lee and G. W. Rubloff, *Nat. Nanotechnol.*, 2009, **4**, 292-296.